Volume 9 | Number 36 | 28 September 2018 | Pages 7161–7288

Chemical Science

rsc.li/chemical-science

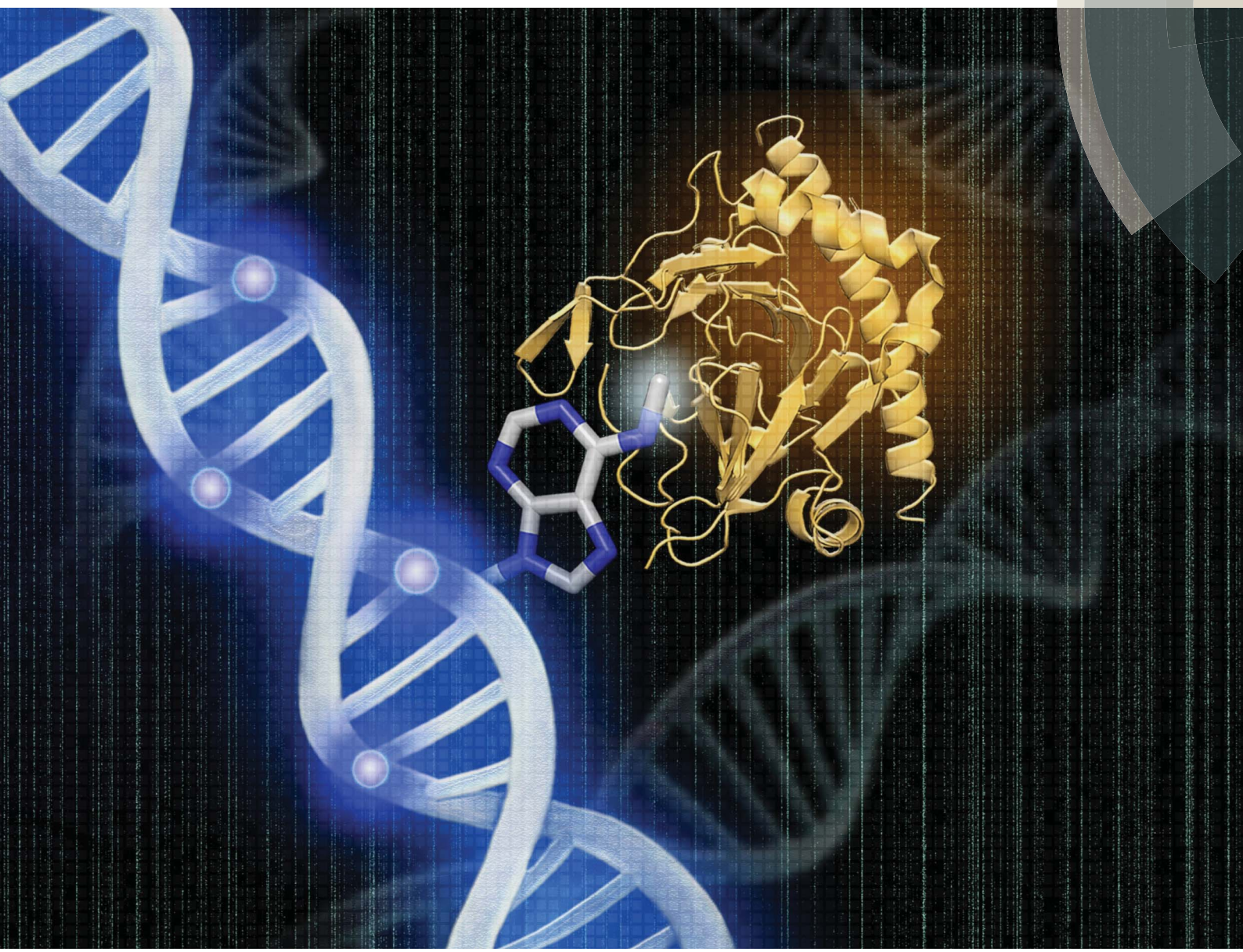

ISSN 2041-6539

ROYAL SOCIETY OF CHEMISTRY

EDGE ARTICLE

Esther C. Y. Woon *et al.*

A fluorescent methylation-switchable probe for highly sensitive analysis of FTO N^6-methyladenosine demethylase activity in cells

Chemical Science

EDGE ARTICLE

View Article Online
View Journal | View Issue

Check for updates

Cite this: *Chem. Sci.*, 2018, **9**, 7174

All publication charges for this article have been paid for by the Royal Society of Chemistry

Open Access Article. Published on 07 August 2018. Downloaded on 7/8/2025 12:55:09 PM.
This article is licensed under a Creative Commons Attribution-NonCommercial 3.0 Unported Licence.

A fluorescent methylation-switchable probe for highly sensitive analysis of FTO N^6-methyladenosine demethylase activity in cells†

Adeline Cheong,[a] Joanne J. A. Low,[a] Andrea Lim,[ab] Paul M. Yen[b] and Esther C. Y. Woon *[a]

Received 16th May 2018
Accepted 1st August 2018

DOI: 10.1039/c8sc02163e

rsc.li/chemical-science

N^6-Methyladenosine (m^6A) is one of the most abundant epigenetic modifications on mRNA. It is dynamically regulated by the m^6A demethylases FTO and ALKBH5, which are currently attracting intense medical interest because of their strong association with several human diseases. Despite their clinical significance, the molecular mechanisms of m^6A demethylases remain unclear, hence there is tremendous interest in developing analytical tools to facilitate their functional studies, with a longer term view of validating their therapeutic potentials. To date, no method exists which permits the analysis of m^6A-demethylase activity in cells. To overcome this challenge, herein, we describe the first example of a fluorescent m^6A-switchable oligonucleotide probe, which enables the direct detection of FTO demethylase activity both *in vitro* and in living cells. The m^6A probe provides a simple, yet powerful visual tool for highly sensitive detection of demethylase activity. Through the use of m^6A-probe, we were able to achieve real-time imaging and single-cell flow cytometry analyses of FTO activity in HepG2 cells. We also successfully applied the probe to monitor dynamic changes in FTO activity and m^6A methylation levels during 3T3-L1 pre-adipocyte differentiation. The strategy outlined here is highly versatile and may, in principle, be adapted to the study of a range of RNA demethylases and, more widely, other RNA modifying enzymes. To the best of our knowledge, the present study represents not only the first assay for monitoring FTO activity in living cells, but also a new strategy for sensing m^6A methylation dynamics.

Introduction

N^6-Methyladenosine (m^6A) is an important post-transcriptional modification that is present in more than half of all mammalian messenger RNAs (mRNAs).[1–3] It is currently of intense chemical and biological interest because of its critical roles in various key cellular processes, such as the regulation of mRNA stability, translation efficiency and alternative splicing.[4–10] In recent years, it has become increasingly clear that the m^6A methylation level in mRNA is dynamically regulated by a complex interplay between the m^6A methyltransferases (MTases), such as the METTL3-METTL14-WTAP complex,[11–13] which catalyse the installation of m^6A modification on mRNA and the m^6A demethylases, such as FTO (fat mass and obesity-associated protein)[14] and ALKBH5 (AlkB homologue 5),[15] which directly remove the m^6A mark *via* an oxidative-demethylation mechanism. Both FTO and ALKBH5 belong to the broader family of iron- and 2-oxoglutarate (2OG)-dependent AlkB dioxygenases which also includes *Escherichia coli* AlkB and eight human homologues, ALKBH1-8.[16–18] There is emerging evidence that the aberrant expression of these m^6A demethylases may underlie the pathogenesis of a number of human diseases. FTO, in particular, is strongly associated with a range of metabolic and neurodegenerative disorders, including obesity,[19] diabetes,[20] non-alcoholic steatohepatitis (NASH)[21] and Alzheimer's diseases,[22] whilst ALKBH5 is likely involved in spermatogenetic defect and male infertility.[15,23] Despite the strong physiological links, the exact molecular mechanisms for the m^6A demethylases remain unclear. Hence there is currently tremendous interest in developing analytical tools to facilitate the functional and mechanistic studies of these enzymes, with a longer term view of validating their therapeutic potentials.

However, the m^6A demethylase activity of FTO and ALKBH5 has proven challenging to assay, especially in cells, in part due to the small size and chemical inertness of the N^6-methyl group they remove. Consequently, at present, only few methods have been reported for their analysis. This includes the detection of demethylated DNA/RNA product using HPLC or MALDI-TOF mass spectrometry,[14,15,24–26] gel electrophoresis of enzyme-

[a]*Department of Pharmacy, National University of Singapore, 18 Science Drive 4, 117543, Singapore. E-mail: esther.woon@nus.edu.sg; Fax: +65 6779 1554; Tel: +65 6516 2932*

[b]*Program of Cardiovascular and Metabolic Disorders, Duke-NUS Medical School, 8 College Road, 169857, Singapore*

† Electronic supplementary information (ESI) available: Experimental details, including full synthesis procedure, protein purification methods, fluorescence and spectroscopic studies, thermodynamic analyses, biochemical and cell-based experimental conditions. See DOI: 10.1039/c8sc02163e

This journal is © The Royal Society of Chemistry 2018

Open Access Article. Published on 07 August 2018. Downloaded on 7/8/2025 12:55:09 PM.
This article is licensed under a Creative Commons Attribution-NonCommercial 3.0 Unported Licence.

digested substrates,[26] fluorescence analysis of fluorescein-labelled ssDNA substrate,[26] immuno-detection with m^{6}A-specific antibodies[14,15,24–26] and, more recently, RNA aptamer-based and MazF endonuclease-based fluorescence assays.[27,28] Whilst these methods are useful, many of them are limited by poor sensitivity, low throughput and incompatibility with live-cell applications. Moreover, to date, no method exists which permits the real-time analysis of m^{6}A-demethylase activities in living cells; this severely hinders the study of these clinically-important enzymes.

We,[29] and others,[30–33] have previously showed that although m^{6}A is able to participate in Watson–Crick base pairing in DNA/RNA duplexes, this is achieved by restricting the N^6-methyl-amino group in an energetically unfavourable *anti*-conformation (with respect to N^1 in the purine ring). Thus the presence of m^{6}A modification has a general destabilising effect on DNA/RNA duplexes and could, in fact, trigger a major overall conformational change in certain sequence contexts. Indeed, m^{6}A has been shown to induce a dramatic duplex–hairpin conversion in some RNA sequences.[29,31] The structure-modifying influence of m^{6}A has also been observed in cellular RNAs, such as human MALAT1 (metastasis associated lung adenocarcinoma transcript 1), where m^{6}A apparently modulates RNA–protein interactions by altering the local RNA structure.[34,35] Inspired by these fascinating observations, we envisaged that m^{6}A-induced conformational change could provide a basis for sensing m^{6}A (de)methylation in cells.

Herein, we describe the first example of a fluorescent m^{6}A-switchable probe, which enables the highly sensitive and selective detection of FTO demethylase activity both *in vitro* and in living cells. The analytical principle is illustrated in Fig. 1a. The m^{6}A-probe is a structurally dynamic oligonucleotide probe which, by design, has the capacity to switch between different conformations according to its m^{6}A methylation status. When the probe is methylated, it preferentially adopts a B-like hairpin structure. Removal of the m^{6}A methyl group by FTO, however, triggers a rapid and spontaneous transformation to an A-duplex. To visualise this conformational change, we employed the pyrene-labelled uridine 2′-*O*-(1-pyrenylmethyl)uridine (U^P; Fig. 1b) as the fluorescent reporter. U^P is particularly suited for our probe design because its fluorescence emission is highly sensitive to its local structural environment. Previous

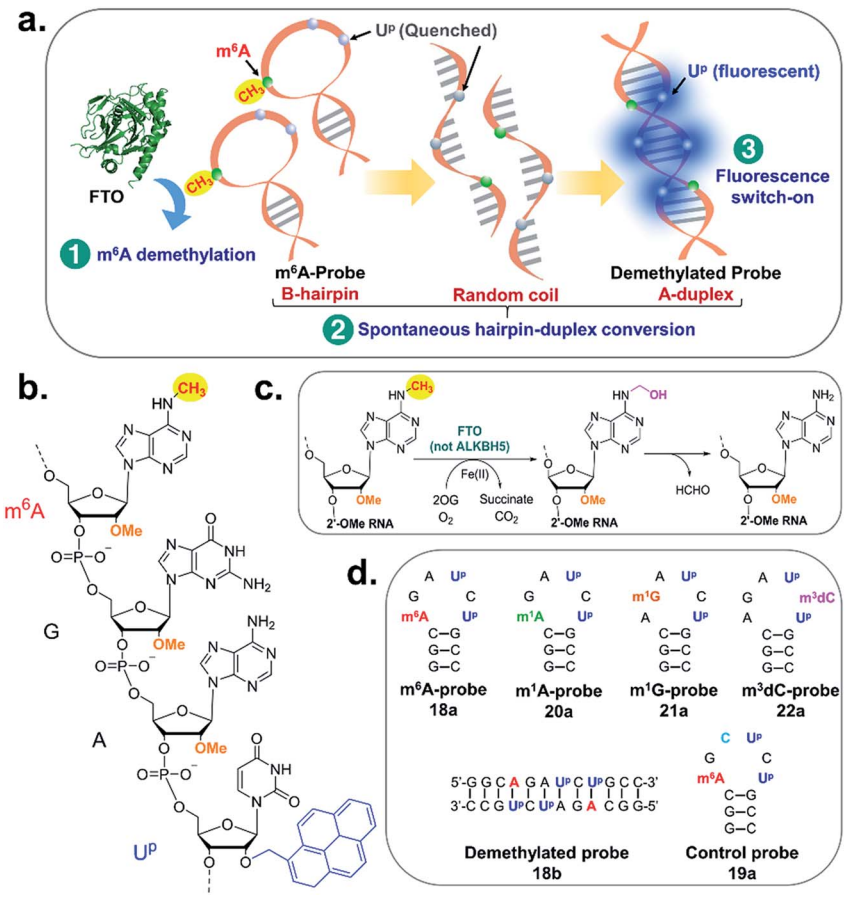

Fig. 1 The fluorescence m^{6}A-switchable probe strategy. (a) The m^{6}A-probe is conformationally-responsive to its m^{6}A methylation status. Removal of m^{6}A methylation by FTO triggers a dramatic switch from hairpin to duplex structure, with concomitant activation of the fluorescent nucleotide 2′-*O*-(1-pyrenylmethyl)uridine (U^P). (b) Structures of U^P and m^{6}A. (c) Proposed mechanism for the demethylation of m^{6}A-probe by FTO. The N^6-methyl group is first oxidised to a hydroxymethyl group, which then fragments spontaneously to give formaldehyde and the demethylated base. ALKBH5 could not demethylate the m^{6}A-probe. (d) Schematic representation of the m^{6}A-probe and its demethylated counterpart. The probe design is highly versatile and could be adapted to the construction of fluorescence-switchable probes containing other nucleic acid base modifications, including N^1-methyladenosine (m^{1}A), N^1-methylguanosine (m^{1}G) and N^3-methylcytosine (m^{3}dC).

Open Access Article. Published on 07 August 2018. Downloaded on 7/8/2025 12:55:09 PM.
This article is licensed under a Creative Commons Attribution-NonCommercial 3.0 Unported Licence.

photophysical studies showed that U^P is quenched when stacked with other nucleobases in a single-stranded or hairpin loop environment due to photo-induced charge transfer from the pyrene to neighbouring nucleobases.[36–39] However it emits brightly when in a compact A-duplex environment due to disposition of pyrene to the non-quenching minor groove.[36–39] Although U^P and other pyrene-modified nucleotides have been widely used to probe DNA/RNA structures, base-flipping and protein–nucleic acid interactions,[36–39] to date, U^P has not been applied to the study of m^6A methylation dynamics. There is also no report of pyrene-based probe that switches fluorescence in response to methylation status.

As we shall demonstrate, the fluorescent m^6A-probe provides a simple, yet powerful visual tool that permits the highly sensitive detection of FTO demethylase activity. Through the use of m^6A-probe, we were able to achieve real-time imaging and single-cell flow cytometry analysis of FTO activity in living cells. We also successfully applied the probe to monitor dynamic changes in FTO activity and m^6A methylation levels during 3T3-L1 pre-adipocyte differentiation. The strategy outlined here is simple, inexpensive and amenable to high-throughput format. It is also highly versatile and may, in principle, be applied to the study of a range of RNA demethylases and, more widely, other RNA modifying enzymes. Prior to this study, there is no report of assay method that enables the direct monitoring of FTO m^6A-demethylase activity in living cells. We are also not aware of any cell-based assay that specifically target FTO over ALKBH5 (the only other human enzyme currently known to demethylate m^6A in RNAs). Hopefully the development of this highly selective approach will advance our understanding of the roles of FTO in m^6A-mediated epigenetic processes and its mechanistic connection to human diseases.

Results and discussion

Design strategy for m^6A-switchable probes

We begin by identifying oligonucleotide sequences that are structurally-responsive to m^6A methylation changes. To engender probes that are sufficiently stable for *in vitro* and live-cell applications, we considered a series of 2′-*O*-methyl RNAs of varying length, each containing a single m^6A modification (Table 1; for details of chemical synthesis, see ESI†). The probes are modelled after the general palindromic sequence 5′-(GCGCGAGCUCGCGC)-3′, which consists of a middle 'AGCU segment' (underlined), flanked on both side by two 'CG segments'. Because of their self-complementary nature, they can inherently form two main conformations in solution, namely (1) duplex structure, by engaging in intermolecular base pairing, and (2) hairpin structure, by folding back on themselves.[40] We hypothesised that, in certain sequence contexts, the introduction of an m^6A modification in the 'middle segment' could significantly disrupt duplex base-pairing, thereby forcing the probe to adopt a hairpin conformation (where m^6A could be stably localised within the hairpin loop). Removal of the m^6A modification, however, is expected to restore full base pairing ability and thus favours the alternative duplex structure.

The m^6A-probe switches between hairpin and duplex conformations according to its methylation status

To test our hypothesis, we first compared the UV-melting profile of each of the methylated probes (**1a–12a**) with that of their non-methylated counterparts (**1b–12b**) to obtain a qualitative picture of the influence of m^6A methylation on their secondary structures (Fig. 2 and S1–S6†). The assignment of hairpin and duplex conformations was initially made based on the hyperchromicity of the melting curves and the dependence of melting temperatures (T_ms) on strand concentration; melting transitions that exhibit low UV hyperchromicity (~10%) and concentration-*independent* T_ms are suggestive of a monomolecular hairpin structure, whereas those that show strong hyperchromicity (~20%) and concentration-*dependent* T_ms are characteristic of a bimolecular duplex structure. The results are summarised in Table 1. Amongst the sequences investigated, probes **8**, **11** and **12** were found to be structurally-responsive towards m^6A methylation status. Consistent with our design strategy, they preferentially adopt a hairpin structure when methylated, but convert to a duplex structure upon removal of the m^6A modification. The transformation of the probe from hairpin to duplex structure appears to be primarily an enthalpy-driven process, as evidenced by the highly favourable enthalpy change (*e.g.* $\Delta\Delta H^\circ$ (**12a** → **12b**) = −56.9 kcal mol^{-1}) which counteracts the large entropy cost ($\Delta\Delta S^\circ$ (**12a** → **12b**) = −145.1 cal mol^{-1} K^{-1}) (Table 1, Fig. S4 and S6†). Moreover, the magnitude of destabilisation caused by a single m^6A base on 2′-*O*-methyl RNA duplexes is relatively small, ranging from 0.4–1.8 kcal mol^{-1}, which is similar to values reported for RNA duplexes (0.35–1.7 kcal mol^{-1}),[29–33] suggesting that m^6A is generally well-accommodated within 2′-*O*-methyl RNA duplexes.

To confirm the observed conformational change, we performed circular dichroism (CD) analysis of probes **8**, **11** and **12**, which clearly revealed a B-like hairpin structure for the methylated probes and an A-form duplex for the corresponding non-methylated equivalents (Fig. 2c and S8†). Native polyacrylamide gel electrophoresis further revealed only one discrete band for each strand, indicating that they exist exclusively as hairpin or duplex structure, rather than a mixture of conformations (Fig. 2d and S8d†). Thus these probes likely undergo complete hairpin–duplex conversion in response to methylation changes. We appreciate that for more vigorous proof of secondary structure, other analytical methods such as 2D NMR studies are required. Nevertheless, data from the present study clearly demonstrated that probes **8**, **11** and **12** have the capacity to spontaneously adopt two distinct conformations according to their methylation status, thus they could potentially function as m^6A-switchable probes for sensing m^6A demethylase activity.

Direct visualisation of methylation changes using pyrene-labelled uridine as the fluorescent reporter

We next investigated whether it is possible to monitor the conformational dynamics of the probe using 2′-*O*-(1-pyrenylmethyl)uridine (U^P) as the fluorescent sensor (Fig. 1b). To identify suitable positions for fluorophore placement, each

 This journal is © The Royal Society of Chemistry 2018

Open Access Article. Published on 07 August 2018. Downloaded on 7/8/2025 12:55:09 PM.
This article is licensed under a Creative Commons Attribution-NonCommercial 3.0 Unported Licence.

Table 1 Sequences of selected 2′-*O*-Me RNA probes investigated in this study and their thermodynamic parameters

	Probe	Sequence	Preferred conformation	T_m[a] (°C) (at 5 μM)	ΔH°[b] (kcal mol^{-1})	ΔS°[b] (cal mol^{-1} K^{-1})	ΔG°_{310} (kcal mol^{-1})
14mer	1a	2′-OMe(GCGCG A^{m6}GCU CGCGC)	Duplex	87.6 ± 0.3	−125.0 ± 1.5	−322.2 ± 1.9	−25.1 ± 0.1
	1b	2′-OMe(GCGCG AGCU CGCGC)	Duplex	90.5 ± 0.3	−131.3 ± 1.5	−336.7 ± 2.5	−26.9 ± 0.1
12mer	2a	2′-OMe(GCCG A^{m6}GCU CGGC)	Duplex	75.4 ± 0.2	−112.3 ± 0.8	−297.9 ± 2.1	−20.0 ± 0.2
	2b	2′-OMe(GCCG AGCU CGGC)	Duplex	78.4 ± 0.5	−117.7 ± 1.0	−310.5 ± 3.0	−21.5 ± 0.2
	3a	2′-OMe(CGCG A^{m6}GCU CGCG)	Duplex	73.5 ± 0.5	−109.0 ± 0.7	−290.2 ± 2.5	−19.2 ± 0.2
	3b	2′-OMe(CGCG AGCU CGCG)	Duplex	75.1 ± 0.3	−113.2 ± 1.2	−300.2 ± 3.4	−20.0 ± 0.1
	4a	2′-OMe(CGGC A^{m6}GCU GCCG)	Duplex	77.4 ± 0.3	−116.9 ± 0.5	−309.2 ± 2.0	−21.2 ± 0.1
	4b	2′-OMe(CGGC AGCU GCCG)	Duplex	80.2 ± 0.2	−119.1 ± 0.9	−312.8 ± 3.6	−22.1 ± 0.1
	5a	2′-OMe(CCGG A^{m6}GCU CCGG)	Duplex	73.8 ± 0.4	−108.8 ± 1.1	−289.3 ± 2.7	−19.1 ± 0.2
	5b	2′-OMe(CCGG AGCU CCGG)	Duplex	76.5 ± 0.5	−117.4 ± 1.0	−311.5 ± 3.1	−20.8 ± 0.2
10mer	6a	2′-OMe(GCC A^{m6}GCU GGC)	Duplex	63.8 ± 0.4	−84.7 ± 1.5	−227.1 ± 2.1	−14.3 ± 0.1
	6b	2′-OMe(GCC AGCU GGC)	Duplex	65.6 ± 0.5	−88.1 ± 1.0	−235.8 ± 2.4	−15.0 ± 0.2
	7a	2′-OMe(GCG A^{m6}GCU CGC)	Duplex	63.6 ± 0.2	−84.1 ± 1.3	−225.5 ± 3.4	−14.2 ± 0.1
	7b	2′-OMe(GCG AGCU CGC)	Duplex	64.2 ± 0.3	−87.4 ± 0.4	−234.8 ± 1.9	−14.6 ± 0.1
	8a	2′-OMe(GGC A^{m6}GCU GCC)	Hairpin	69.2 ± 0.5	−36.9 ± 1.5	−107.8 ± 3.6	−3.5 ± 0.2
	8b	2′-OMe(GGC AGCU GCC)	Duplex	65.3 ± 0.5	−89.5 ± 0.7	−240.2 ± 2.1	−15.0 ± 0.2
	9a	2′-OMe(CCG A^{m6}GCU CGG)	Duplex	60.9 ± 0.4	−80.5 ± 0.8	−216.7 ± 2.8	−13.3 ± 0.1
	9b	2′-OMe(CCG AGCU CGG)	Duplex	63.2 ± 0.2	−82.4 ± 0.9	−220.7 ± 2.1	−14.0 ± 0.2
	10a	2′-OMe(CGG A^{m6}GCU CCG)	Duplex	61.7 ± 0.5	−83.8 ± 1.2	−226.0 ± 3.4	−13.7 ± 0.1
	10b	2′-OMe(CGG AGCU CCG)	Duplex	65.5 ± 0.2	−87.4 ± 1.0	−233.8 ± 2.5	−14.9 ± 0.1
Analogues of 8	11a	2′-OMe(GGC A^{m6}GUACU GCC)	Hairpin	73.1 ± 0.2	−42.0 ± 0.6	−121.3 ± 2.7	−4.4 ± 0.1
	11b	2′-OMe(GGC AGUACU GCC)	Duplex	67.8 ± 0.3	−99.4 ± 1.1	−267.3 ± 3.5	−16.5 ± 0.1
	12a	2′-OMe(GGC A^{m6}GAUCU GCC)	Hairpin	73.5 ± 0.4	−41.6 ± 0.7	−120.0 ± 1.7	−4.4 ± 0.2
	12b	2′-OMe(GGC AGAUCU GCC)	Duplex	67.3 ± 0.3	−98.5 ± 1.4	−265.1 ± 3.1	−16.3 ± 0.1
	18a (m^6A-probe)	2′-OMe(GGC A^{m6}GAU^{P}CU^{P} GCC)	Hairpin	72.2 ± 0.5	−42.3 ± 1.3	−122.5 ± 2.5	−4.3 ± 0.2
	18b (demethylated probe)	2′-OMe(GGC AGAU^{P}CU^{P} GCC)	Duplex	65.2 ± 0.4	−97.9 ± 0.5	−265.2 ± 3.8	−15.7 ± 0.2
	19a (control probe)	2′-OMe(GGC A^{m6}GCU^{P}CU^{P} GCC)	Hairpin	71.4 ± 0.8	−40.5 ± 1.5	−117.3 ± 1.3	−4.1 ± 0.2
	19b	2′-OMe(GGC AGCU^{P}CU^{P} GCC)	Hairpin	71.8 ± 0.3	−41.2 ± 1.7	−119.4 ± 2.4	−4.2 ± 0.2

[a] Melting temperature (T_m) was determined by UV melting analysis at 5 μM total strand concentration (in 10 mM sodium phosphate buffer containing 150 mM NaCl, pH 7.4). [b] ΔH° and ΔS° values for duplexes were determined from $1/T_m$ *versus* ln(strand concentration) plot, whilst that of hairpins were obtained from α (the fraction of strands remaining hybridised) *versus* temperature plot by curve fitting to a two-state transition model.

uridine residue in probes **8**, **11** and **12** was systematically replaced with a U^P residue. Fluorescence analysis (λ_{ex} 340 nm) of the resulting probes **13–17** (Table S2†) indicates that U^P emission is most effectively quenched (*via* PET) when incorporated at the U^7 or U^9 positions of probe **12** (Fig. 3, S9 and S10†). This gives starting methylated probes with very low fluorescence quantum yields (Φ_F) of 0.04 (**16a**) and 0.06 (**17a**), respectively. Their non-methylated counterparts, **16b** and **17b**, however, are brightly fluorescent (Φ_F 0.24 and 0.25) and exhibit at least 4-fold greater fluorescence intensity.

Open Access Article. Published on 07 August 2018. Downloaded on 7/8/2025 12:55:09 PM.
This article is licensed under a Creative Commons Attribution-NonCommercial 3.0 Unported Licence.

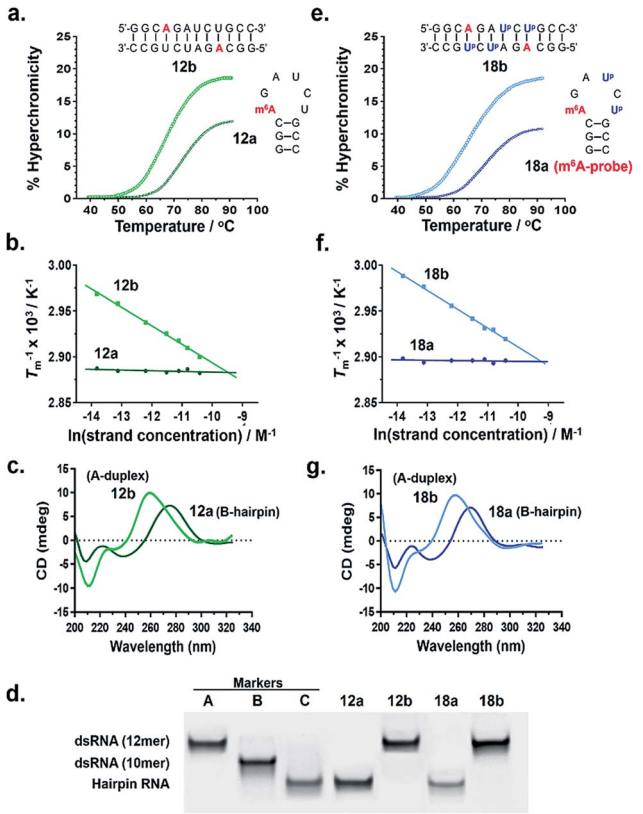

Fig. 2 Verification of the m^{6}A-probe design. Both probe **12a** and its U^P-labelled analogue **18a** (m^{6}A-probe) are able to spontaneously adopt two distinct conformations (hairpin or duplex) in response to their m^{6}A methylation status, as demonstrated by their (a, e) UV melting profiles, (b, f) van't Hoff plots, (c, g) CD spectra, and (d) native polyacrylamide gel. All UV and CD experiments were performed at 5 μM strand concentration in 10 mM sodium phosphate buffer containing 150 mM NaCl, pH 7.4. Gel marker A: 12mer dsRNA r(CGCGCGCGCGCG);[2] marker B: 10mer dsRNA r(CGCGCGCGCG);[2] marker C: 12mer hairpin RNA (CGCGAAUUCGCG). For the conformational analyses of probes **8a** and **11a**, see Fig. S8.†

Due to the modular nature of our probe design, it is possible to further amplify the fluorescence signal of the probe through judicious placement of several U^P monomers, as exemplified by **18a** where the concurrent incorporation of two U^P residues led to a dramatic increase in fluorescence light-up response ($\Delta\Phi_F \sim$ 12-fold; $\varepsilon_{340} = 9.4 \times 10^4$ M^{-1} cm^{-1}), with concomitant appearance of a broad excimer emission peak at ~475 nm (Fig. 3b). We appreciate that the presence of bulky U^P residue might alter the hairpin conformation of **18a**, nevertheless, our results from UV-melting, CD and native PAGE analyses revealed little or no change in its overall secondary structure compared with parent probe **12a** (Fig. 2 and S7†). The non-methylated equivalent **18b** also retained the ability to dimerise into stable A-duplex structure ($\Delta G^\circ_{310} = -15.7$ kcal mol^{-1}; Table 1).

Taken together, these results demonstrated that it is possible to visualise methylation changes in the probe using U^P as the fluorescent reporter. Because **18a** gave the greatest fluorescence switch-on response and signal-to-noise ratio, it was selected as our representative m^{6}A-probe for further investigation.

The m^{6}A-probe enables highly sensitive detection of FTO demethylase activity

We first examined whether the m^{6}A-probe could serve as fluorogenic substrate for FTO. In our *in vitro* m^{6}A-probe assay, 10 μM of the probe was incubated with FTO (0.5 μM) in the presence of Fe(II) (cofactor; 100 μM), 2-oxoglutarate (2OG; cosubstrate; 100 μM) and L-ascorbate (2 mM) under physiologically-relevant conditions (50 mM HEPES buffer, pH 7.4, 37 °C). The fluorescence of the reaction (λ_{ex} 340 nm) was monitored over time and the emergence of fluorescent demethylated probe **18b** was indicated by an increase in emission at 410 nm. As shown in Fig. 4a, strong fluorescence could be detected within 30 min of incubation, suggesting that the probe was readily demethylated by FTO. Maximum signal was reached in approximately 2 h, giving a ~10-fold increase in fluorescence intensity. Such a large fluorescence light-up response is remarkable considering only a single methyl group change between the probe and the demethylated product. Thus the use of m^{6}A-probe enables highly sensitive detection of FTO demethylase activity.

Consistent with fluorescence analysis, HPLC analysis of the reaction mixture at various time points showed a time-dependent increase in formation of demethylated product with concomitant decrease in m^{6}A-probe level (Fig. 4c–f). Moreover, the product concentration correlates linearly with the fluorescence intensity (Fig. 4j), hence the fluorescence signal provides a direct indication of FTO demethylase activity.

To confirm that the observed fluorescence increase was specifically triggered by FTO demethylase activity and not due to auto-fluorescence or other non-specific mechanisms, we repeated the m^{6}A-probe assay using an FTO missense mutant, FTO^{R316Q}, which has significantly reduced (80% less) demethylase activity.[14] As anticipated, FTO^{R316Q} gave a greatly diminished fluorescence response compared with wild-type FTO, clearly demonstrating that fluorescence activation was indeed induced by FTO-dependent demethylase activity (Fig. 4a and g). Consistent with this finding, control experiments lacking FTO or any of the key assay components *i.e.* 2OG (cosubstrate) or Fe(II) (cofactor) did not result in any fluorescence increase (Fig. S12†). Subsequent kinetic analysis using a HPLC-based assay revealed that the m^{6}A-probe is a reasonably good substrate for FTO ($k_{cat}/K_m = 1.05$ min^{-1} μM^{-1}; Fig. 4k and S11†), and could, in fact, be demethylated with similar efficiency as ssRNA and ssDNA substrates containing the GG(m^{6}A)CU consensus motif. This result is interesting because it suggests that, in addition to DNA and RNA substrates, FTO is also able to demethylate m^{6}A modification residing on 2′-*O*-methyl RNAs, consistent with recent report that FTO demethylates N^6,2′-*O*-dimethyladenosine (m^{6}A$_m$) modification in the 5′ cap of mRNA.[46]

To further explore whether the hairpin–duplex structural change is truly essential for probe fluorescence activation, we prepared control probe **19a**-an analogue of m^{6}A-probe wherein the adenine base at position 6 was replaced with cytosine (Fig. 1d). This single base substitution renders the control probe non-palindromic, thus unable to undergo hairpin–duplex conversion on demethylation, as verified by UV-melting analysis (Table 1 and Fig. S7†). Treatment of the control probe with FTO

This journal is © The Royal Society of Chemistry 2018

Open Access Article. Published on 07 August 2018. Downloaded on 7/8/2025 12:55:09 PM.
This article is licensed under a Creative Commons Attribution-NonCommercial 3.0 Unported Licence.

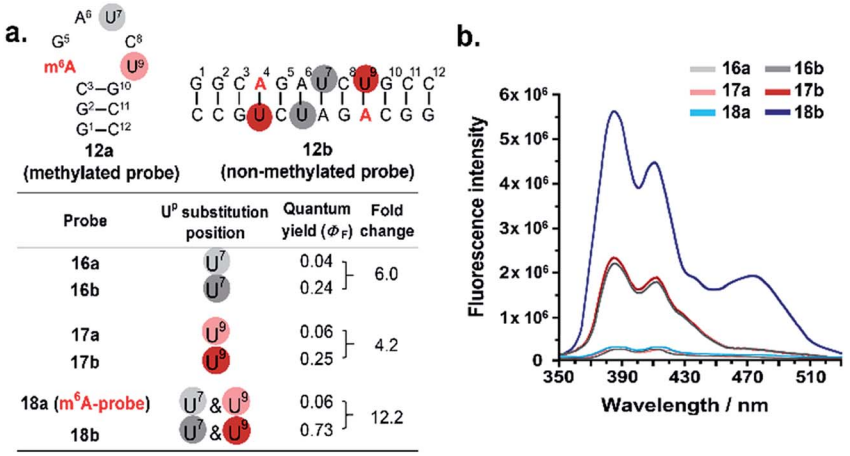

Probe	U^P substitution position	Quantum yield (Φ_F)	Fold change
16a	U^7	0.04	6.0
16b	U^7	0.24	
17a	U^9	0.06	4.2
17b	U^9	0.25	
18a (m^6A-probe)	U^7 & U^9	0.06	12.2
18b	U^7 & U^8	0.73	

Fig. 3 Effects of U^P substitution position on fluorescence light-up response. (a) Uridine residues at U^7 and U^9 positions of probes **12a** and **12b** (colour coded) were systematically replaced with the fluorescence nucleotide U^P to generate probes **16–18**. (b) The fluorescence emission spectra (λ_{ex} 340 nm) of the probes were recorded at 5 μM strand concentration under physiologically-relevant conditions (10 mM sodium phosphate buffer containing 150 mM NaCl, pH 7.4, 37 °C). Two pyrene emission peaks at λ_{em} ~385 nm and ~410 nm were observed. The concurrent placement of two U^P residues at U^7 and U^9 positions *i.e.* **18a** (m^6A-probe) led to a dramatic ~12-fold enhancement in fluorescence light-up response, with concomitant appearance of a broad excimer emission peak at ~475 nm. The fluorescence quantum yields were determined with ±10% accuracy. For the effects of U^P substitution on probes **8** and **11**, see Fig. S9 and S10.†

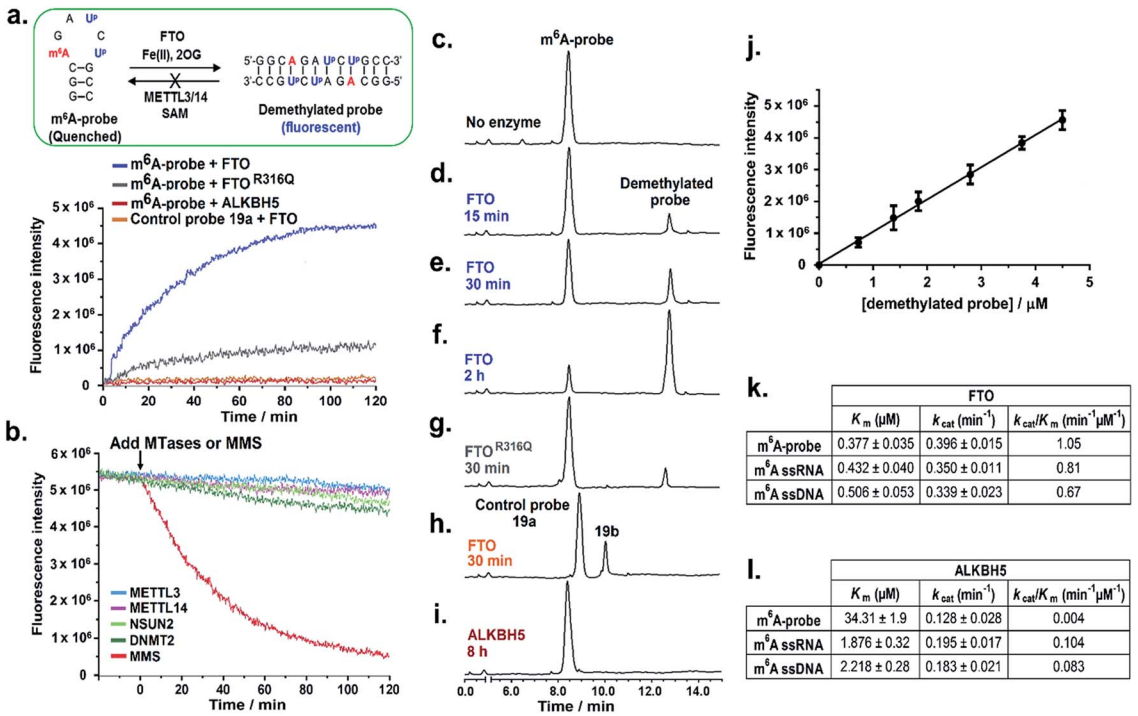

k.

	FTO		
	K_m (μM)	k_{cat} (min^{-1})	k_{cat}/K_m ($min^{-1}\mu M^{-1}$)
m^6A-probe	0.377 ± 0.035	0.396 ± 0.015	1.05
m^6A ssRNA	0.432 ± 0.040	0.350 ± 0.011	0.81
m^6A ssDNA	0.506 ± 0.053	0.339 ± 0.023	0.67

l.

	ALKBH5		
	K_m (μM)	k_{cat} (min^{-1})	k_{cat}/K_m ($min^{-1}\mu M^{-1}$)
m^6A-probe	34.31 ± 1.9	0.128 ± 0.028	0.004
m^6A ssRNA	1.876 ± 0.32	0.195 ± 0.017	0.104
m^6A ssDNA	2.218 ± 0.28	0.183 ± 0.021	0.083

Fig. 4 The m^6A-probe is remarkably selective for FTO over ALKBH5. (a) Time-course fluorescence analyses (λ_{ex} 340 nm; λ_{em} 410 nm) of the m^6A-probe (10 μM) in the presence of FTO (0.5 μM), FTO^{R316Q} (0.5 μM), and ALKBH5 (2 μM) showed that probe fluorescence is activated solely by FTO and not by ALKBH5. (b) There was no appreciable change in the fluorescence intensity (λ_{em} 410 nm) of the demethylated probe when exposed to m^6A MTases (METTL3 and METTL14) and m^5C MTases (NSUN2 and DNMT2), implying no re-methylation of the demethylated probe by these MTases. Treatment with methyl methanesulfonate (MMS) however caused a significant decline in fluorescence. HPLC analysis of m^6A-probe (c) in the absence of enzyme (control), and after treatment with FTO for (d) 15 min, (e) 30 min, and (f) 2 h. There was a time-dependent increase in formation of demethylated product with a concomitant decrease in m^6A-probe substrate. Treatment of m^6A-probe with (g) FTO^{R316Q}, (h) control probe **19a**, and (i) ALKBH5. The assignment of HPLC peaks was made by comparison with known standards. (j) There is an excellent linear relationship between the fluorescence intensity of the demethylated probe and its concentration. Data are expressed as mean ± SD of three replicates. Kinetic parameters for the demethylation of m^6A-probe, m^6A-ssRNA (5′-GCGG-m^6A-CUCCAGAUG-3′) and m^6A-ssDNA (5′-GCGG-m^6A-CTCCAGATG-3′) by (k) FTO and (l) ALKBH5.

Open Access Article. Published on 07 August 2018. Downloaded on 7/8/2025 12:55:09 PM.
This article is licensed under a Creative Commons Attribution-NonCommercial 3.0 Unported Licence.

failed to produce any fluorescence increase (Fig. 4a) despite clear evidence of demethylated product formation by HPLC analysis (Fig. 4h). Thus, fluorescence turn-on is strictly dependent on a switch in probe conformation from hairpin to duplex structure.

The m^{6}A-probe is remarkably selective for FTO over ALKBH5 and other subfamily members

We next evaluated the specificity of the m^{6}A-probe by testing it against several FTO subfamily members, namely ALKBH2,[41–43] ALKBH3 [43,44] and ALKBH5.[15,45] These enzymes are of particular interest because they not only share high levels of sequence and structural homology with FTO, but also possess direct nucleic acid demethylase activities.[25] The results from HPLC-based and fluorescence assays showed negligible demethylated product formation and fluorescence activation for all enzymes investigated, suggesting that the m^{6}A-probe is highly selective for FTO over its subfamily members (Fig. S12†). The apparent lack of fluorescence response towards ALKBH5 is notable because ALKBH5 is also known to demethylate m^{6}A on mRNAs (Fig. 4a and l). Such exceptional selectively renders the probe potentially useful for studying the respective roles of FTO and ALKBH5 in m^{6}A-mediated epigenetic processes. The mechanism by which the m^{6}A-probe discriminates against ALKBH5 is unclear at present, however, in light that ALKBH5 could effectively demethylate the RNA equivalent of the m^{6}A-probe, selectivity is likely attributed to the 2′-*O*-methyl backbone.

Besides selectivity, the m^{6}A-probe also exhibits excellent sensitivity and dynamic range. Titration of the probe (10 μM) with decreasing concentrations of FTO indicated that m^{6}A demethylase activity could be detected at FTO concentration as low as 10 nM (Fig. S13†). This is at least a 100-fold more sensitive than conventional assay performed under similar conditions, where micromolar enzyme concentrations are typically required.

The m^{6}A-probe is not methylated by m^{6}A MTases and is highly stable in cell lysate

One potential concern with the use of m^{6}A-probe in cells is that the demethylated probe could, in principle, be re-methylated back to the hairpin structure by cellular m^{6}A methyltransferases (MTases), leading to a reversal of fluorescence activation. To investigate this possibility, we assayed the demethylated probe against METTL3 and METTL14,[11–13] which are the only two m^{6}A MTases identified to date. We also tested it against m^{5}C RNA MTases, NSUN2 [47,48] and DNMT2,[49] to examine for possible methylation on the 'CG segment' of the probe. Interestingly, in all cases, there was no methylation of the demethylated probe, even after prolonged incubation (8 h), as determined by MALDI-TOF MS analysis (Fig. S14†); there was also no appreciable change in the fluorescence intensity of the probe (Fig. 4b). In sharp contrast, control experiment using the methylating agent methylmethane sulfonate (MMS) resulted in a rapid decline in fluorescence signal, suggesting that probe fluorescence could indeed be reversed by methylation (Fig. 4b). Recent studies suggested that many of the MTases exhibit strict sequence and/or structural requirements for substrate recognition. The m^{6}A MTases for instance specifically recognise and bind to the GG(m^{6}A)CU consensus motif.[11–13] This may explain, at least in part, the apparent lack of methylation of the demethylated probes by these enzymes.

To investigate the potential loss of probe fluorescence due to other nucleic acid modifying enzymes or cellular nucleases, we further performed time-course fluorescence analysis of the m^{6}A-probe in HepG2 cell lysate, where FTO is abundantly expressed.[21] As shown in Fig. S15,† the demethylated probe product formed rapidly in cell lysate where it remained strongly emissive for at least 24 h with no obvious decline in fluorescence. This suggests that the probe has good photostability and is fairly resistant to nuclease degradation. Our combined results, therefore, established m^{6}A-probe as a highly sensitive and selective probe suitable for visualising FTO demethylase activity in cells.

The m^{6}A-probe assay enables high-throughput screening of FTO inhibitors

On the basis of these promising data, we next investigated whether the developed m^{6}A-probe assay could be applied to the high-throughput screening of FTO inhibitor. To assess the performance of our assay, a set of structurally-diverse small molecules (Fig. 5a) consisting of known FTO inhibitors (24PDCA,[50] LipotF,[25] Rhein,[24] IOX3 [50]) and non-inhibitor

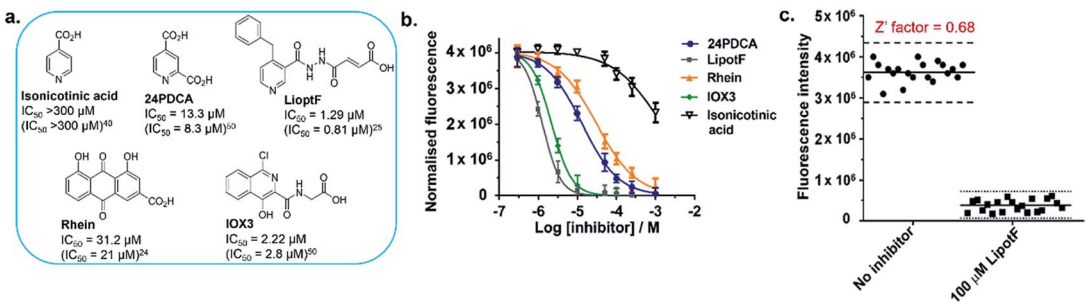

Fig. 5 The m^{6}A-probe assay provides a robust method for the high-throughput screening of FTO inhibitors. (a) Structures of reported FTO inhibitors. The determined IC_{50}s were comparable with previously reported values (in parentheses). (b) Enzyme inhibition curves for the FTO inhibitors, as determined using the m^{6}A-probe assay. Percent enzyme activity was calculated by normalising to the fluorescence signal without inhibitor (100%) and without m^{6}A-probe (0%). Data are expressed as mean ± SD of three replicates. (c) The *Z*′ factor for the m^{6}A-probe assay was determined in a 384-well format, using the method described by Zhang *et al.*[51] A total of 40 independent assays were run with either LipotF (positive control) or DMSO (negative control).

This journal is © The Royal Society of Chemistry 2018

Open Access Article. Published on 07 August 2018. Downloaded on 7/8/2025 12:55:09 PM.
This article is licensed under a Creative Commons Attribution-NonCommercial 3.0 Unported Licence.

isonicotinic acid[40] were individually incubated at various concentrations with FTO (50 nM) and m^{6}A-probe (10 μM) in a 384-well plate, and their fluorescence spectra simultaneously recorded on a fluorescence microplate reader. The inhibition curves are shown in Fig. 5b. With the exception of isonicotinic acid, all compounds investigated induced a clear dose-dependent decrease in fluorescence intensity. The determined IC_{50}s are also comparable with previously reported values (Fig. 5a), thus the m^{6}A-probe assay is able to successfully identify FTO inhibitors across diverse chemical scaffolds. To further evaluate the quality and reproducibility of our m^{6}A-probe assay for screening in a 384-well format, we determined the Z' factor using the method described by Zhang *et al.*[51] (for experimental details, see ESI†). The average Z' factor for our assay was found to be 0.68, which indicates excellent statistical reliability (Fig. 5c). Taken together, the results validate our m^{6}A-probe assay as a robust method for high-throughput screening of FTO inhibitors.

The m^{6}A-probe enables real-time monitoring of FTO activity in living cells

We next proceeded to explore the utility of the m^{6}A-probe for imaging FTO activity in live-cells. To this end, 10 μM of the m^{6}A-probe or control probe **19a** was delivered into HepG2 cells *via* streptolysin-*O* (SLO) reversible permeabilisation method[52] and then analysed using fluorescence microscopy; it has been suggested that this method is more rapid and efficient compared with conventional transfection methods.[52] Preliminary experiments in our lab further showed that SLO-permeabilisation is an effective method for m^{6}A-probe delivery and that SLO treatment does not significantly affect FTO expression in HepG2 cells (Fig. S16†). As shown in Fig. 6a and b, bright blue fluorescence could be observed within the cells after 1 h incubation. This represents a 7-fold increase in fluorescence relative to the control probe (Fig. 6c), which is fairly substantial considering suboptimal filter settings (λ_{ex} 340–380 nm; λ_{em} 435–485 nm).

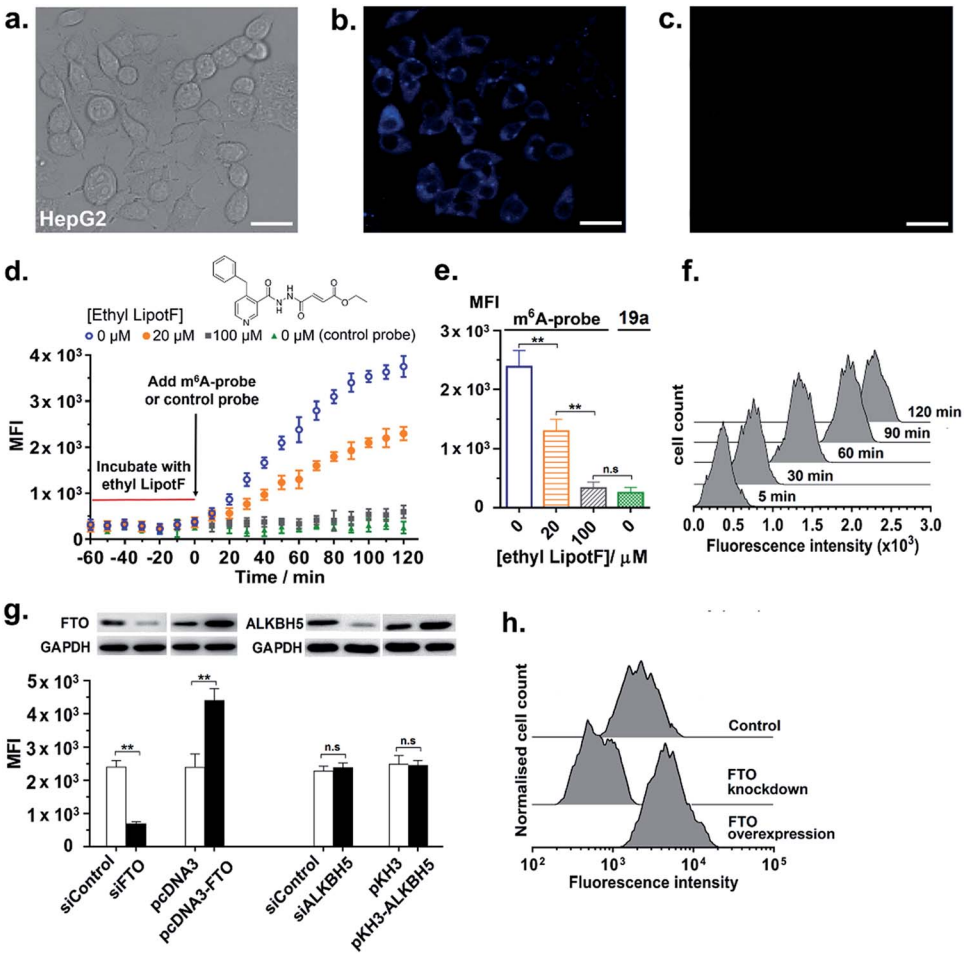

Fig. 6 The m^{6}A-probe enables real-time monitoring of FTO demethylase activity in living cells. Correlated (a) bright field and (b) fluorescent images of HepG2 cells after 1 h treatment with m^{6}A-probe (10 μM; λ_{ex} 340–380 nm; λ_{em} 435–485 nm). (c) Negligible fluorescence was observed for cells treated with control probe **19a** (10 μM). The image in (c) is from a different experiment than the paired images in (a) and (b). Scale bar, 50 μm. (d) Time-course flow cytometry analysis of FTO inhibition in HepG2 cells. Cells were incubated with various concentrations of ethyl LipotF (0, 20 and 100 μM; colour coded) for 1 h before treatment with m^{6}A-probe. MFI is the mean fluorescence intensity of at least 20 000 live cells (λ_{ex} 355 nm; λ_{em} 379 nm). (e) A plot of MFI at 60 min showed a clear dose-dependent decrease in fluorescence intensity. (f) A set of representative flow cytometry profiles for cells treated with 20 μM ethyl LipotF. (g, h) Fluorescence responses of m^{6}A-probe to different FTO and ALKBH5 expression levels in HepG2 cells. The probe responds only to changes in the levels of FTO and not ALKBH5. GAPDH was used as loading control. Data are expressed as mean ± SD of three biological replicates. *P < 0.05; **P < 0.01; n.s = not significant.

Open Access Article. Published on 07 August 2018. Downloaded on 7/8/2025 12:55:09 PM.
This article is licensed under a Creative Commons Attribution-NonCommercial 3.0 Unported Licence.

Notably, the fluorescence appears to accumulate in the cytoplasm, with little or no detectable signal in the nucleus (Fig. S17†). In light of emerging evidence suggesting that FTO shutters between the nucleus and the cytoplasm where it likely serves different cellular functions,[53–55] the selective distribution of m^{6}A-probe in the cytoplasm may allow us to specifically study FTO activity on cytoplasmic mRNAs. Despite toxicity concerns associated with the use of pyrene-based fluorophore in general, MTT cytotoxicity assays showed that the m^{6}A-probe is reasonably well-tolerated by HepG2 and 3T3-L1 cells, with >80% of the cells remaining viable after treatment with 50 μM probe for 24 h (Fig. S18†). The probe also did not significantly affect FTO expression in cells (Fig. S16†).

In addition to live-cell imaging, we further demonstrated that the m^{6}A-probe is compatible with flow cytometry analysis (λ_{ex} 355 nm; λ_{em} 379 nm) and could provide real-time monitoring of FTO inhibition in cells. As shown in the time-course flow cytometry profiles (Fig. 6d–f), incubation of HepG2 cells with various concentrations of ethyl LipotF (a cell-permeable FTO inhibitor developed in our lab; PubChem ID: 126970770)[25] for 1 hour prior to the addition of m^{6}A-probe led to a dose-dependent reduction in fluorescence signal. The control probe **19a**, however, did not produce any fluorescence change, as anticipated.

Flow cytometry experiment further demonstrated that the m^{6}A-probe is highly sensitive towards changes in cellular FTO expression levels. In particular, stable overexpression of FTO in HepG2 cells caused a profound increase in probe fluorescence, whilst FTO knockdown *via* transient transfection with FTO-specific siRNA led to a significant reduction in emission (Fig. 6g, h and S19†). The fluorescence intensity was unchanged with ALKBH5 overexpression or knockdown, thus, consistent with our *in vitro* data, the m^{6}A-probe is exclusively activated by FTO and not by ALKBH5. The m^{6}A-probe therefore provides a single assay platform that permits applications both *in vitro* and in living cells.

The m^{6}A-probe provides a powerful tool for following dynamic changes in endogenous FTO level during cellular differentiation

It is increasingly clear that both FTO expression level and m^{6}A methylation pattern are dynamically regulated during cellular differentiation[7,56] and pathological processes, such as tumourigenesis,[57] DNA damage,[58] heat shock[59] and stress responses.[60] Recent study by Zhao *et al.* in particular showed that FTO expression levels decreased during 3T3-L1 pre-adipocyte FTO FTO expression levels decreased during 3T3-L1

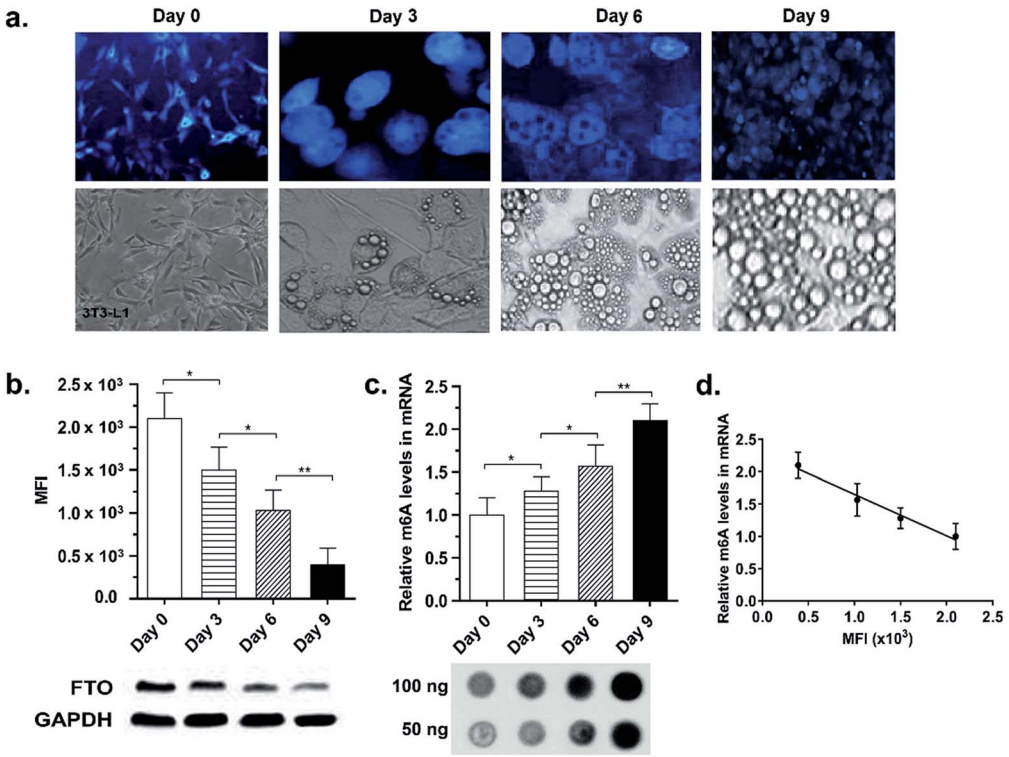

Fig. 7 The m^{6}A-probe provides a powerful tool for following dynamic changes in endogenous FTO activity during cellular differentiation. Differentiation of 3T3-L1 pre-adipocyte was induced by incubation with the differentiation cocktail (IBMX/DEX/Insulin) on Day 0. Cells at different time points of adipogenesis (Day 0, 3, 6, 9) were treated with m^{6}A-probe (10 μM), then analysed with fluorescence microscopy and flow cytometry. (a) Correlated bright field (top panel) and fluorescence (bottom panel) images of 3T3-L1 cells during different phases of adipogenesis. (b) Flow cytometry analysis showed a clear time-dependent decrease in probe fluorescence, suggesting a reduction in FTO activity during adipogenesis. MFI is the mean fluorescence intensity of at least 20 000 live cells (λ_{ex} 355 nm; λ_{em} 379 nm). Data are expressed as mean ± SD of three biological replicates. *P < 0.05; **P < 0.01. (c) The level of m^{6}A in mRNA during different stages of adipogenesis was determined by dot-blot analysis with m^{6}A antibody and quantified by Grayscale analysis with ImageJ software. (d) The observed decreased in fluorescence was accompanied with an increase in m^{6}A levels in mRNA, thus fluorescence signal provides a direct read-out of cellular FTO activity.

This journal is © The Royal Society of Chemistry 2018

Open Access Article. Published on 07 August 2018. Downloaded on 7/8/2025 12:55:09 PM.
This article is licensed under a Creative Commons Attribution-NonCommercial 3.0 Unported Licence.

pre-adipocyte differentiation and this correlated inversely with global m^{6}A levels.[7] We were therefore interested in exploring whether the m^{6}A-probe is able to report dynamic changes in endogenous FTO activity during cellular differentiation. To this end, 3T3-L1 pre-adipocytes were treated with the probe at different time points of adipogenesis *i.e.* Day 0 (prior to treatment with mitotic inducing agent), 3, 6, and 9 and then analysed by fluorescence microscopy and flow cytometry. Consistent with the above-mentioned report,[7] cells on Day 3, 6, and 9 of differentiation exhibited a 1.4-, 2.0- and 5.4-fold decrease in fluorescence intensity, respectively, relative to Day 0 (Fig. 7a and b), suggesting a time-dependent reduction in FTO level and/or activity during adipogenesis. Remarkably, the observed fluorescence decrease also corresponds to a 1.3-, 1.6-, and 2.1-fold increase in m^{6}A levels in mRNAs, respectively, as determined by dot-blot analysis (Fig. 7c and d). Thus the fluorescence intensity provides a direct read-out of cellular FTO activity. Taken together, the results showed that our m^{6}A-probe can provide a simple, yet highly sensitive tool for following dynamic changes in cellular FTO activity.

The m^{6}A-probe strategy could be adapted to the study of a range of nucleic acid modifications

Because our m^{6}A-probe design exploits the universal principle of Watson–Crick base pairing, it may conceptually be applied to the construction of fluorescent switchable-probes for other nucleic acid modifications. To explore the general utility of our probe strategy, we further prepared analogues of m^{6}A-probe containing other physiologically-relevant base modifications, namely N^1-methyladenosine (m^{1}A; an epigenetic modification in mRNAs),[61] N^1-methylguanosine (m^{1}G; a post-transcriptional modification on bacterial rRNA and tRNA)[62] and N^3-methylcytosine (m^{3}dC; a DNA base lesion)[63] (Fig. 1d). Remarkably, the removal of these modified bases triggered a similar hairpin–duplex conformational change, as demonstrated by CD analysis (Fig. S20†). The observed conformational change was again accompanied with significant fluorescence light-up responses ($\Delta\Phi_F$ > 9; Fig. S20d†). Thus our m^{6}A-probe strategy is highly versatile and could potentially be adapted to the study of a range of nucleic acid-modifying enzymes.

Conclusions

Overall, we have provided proof of principle that a novel strategy employing fluorescent m^{6}A-switchable probe could enable highly sensitive detection of FTO m^{6}A-demethylase activity both *in vitro* and in living cells. The developed m^{6}A-probe assay is simple, inexpensive and permits the direct analysis of FTO activity without recourse to radioactive substrates or cumbersome techniques. This assay also requires only small amount of protein (low nanomolar concentrations), thus avoiding the drawbacks of high protein consumption and limited dynamic range associated with current assay methods. Through the use of the m^{6}A-probe, the removal of a single methyl group is dramatically amplified (~10-fold). This enables highly sensitive detection of FTO demethylase activity.

Importantly, the m^{6}A-probe provides a powerful visual tool for direct imaging and single-cell flow cytometry analysis of FTO activity. In this study, we have successfully applied the probe to the real-time monitoring of FTO inhibition in HepG2 cells. We also demonstrated that the m^{6}A-probe is highly sensitive towards cellular FTO expression levels and could report on subtle changes in FTO activity during 3T3-L1 pre-adipocyte differentiation. Thus the m^{6}A-probe may provide insights into the dynamic regulation of cellular processes by FTO. We further showed that the m^{6}A-probe strategy can be applied to the screening of FTO inhibitors across diverse chemical scaffolds. Given the very high level of current interest in FTO as an m^{6}A 'eraser' and as disease target, the development of a single assay platform that allows both the functional study of FTO and the high-throughput discovery of FTO therapeutic leads shall be of significant biological and medical interest.

One limitation of this approach is that, as oppose to genetically-encoded sensors, it is necessary to deliver the m^{6}A-probe into cells exogenously, and this introduces additional handling steps. The probe delivery efficiency also likely varies between different cell types. Moreover, this method is not suitable for base modifications that do not significantly impact duplex stability, such as 5-methylcytosine (m^{5}C) and N^7-methylguanosine (m^{7}G). Nevertheless, the strategy outlined here should be applicable to the wide number of other base modifications that are known to disrupt duplex base pairing. Indeed, we have demonstrated that probes containing modifications, such as m^{1}A, m^{1}G and m^{3}dC also undergo spontaneous hairpin–duplex transformation, with concomitant fluorescence activation. Hence the developed assay could, in principle, be adapted to the study of a range of nucleic acid-modifying enzymes.

Prior to this study, there is no report of assay method that enables the direct analysis of FTO m^{6}A-demethylase activity in living cells. We are also not aware of any cell-based assay that selectively target FTO over ALKBH5 (the only other human enzyme currently known to demethylate m^{6}A in RNAs). The development of this highly selective approach may prove valuable in dissecting the respective roles of FTO and ALKBH5 in m^{6}A-mediated epigenetic processes, which hopefully will advance our understanding of mechanistic links between FTO and human diseases.

Conflicts of interest

The authors declare no competing financial interest.

Acknowledgements

This work was supported by the Singapore Ministry of Health's National Medical Research Council (NMRC/BNIG/2008/2013) and the Singapore Ministry of Education (AcRF Tier 1 Grant R148-000-231-114 and R148-000-238 114).

Notes and references

1 D. Dominissini, S. Moshitch-Moshkovitz, S. Schwartz, M. Salmon-Divon, L. Ungar, S. Osenberg, K. Cesarkas,

Open Access Article. Published on 07 August 2018. Downloaded on 7/8/2025 12:55:09 PM. This article is licensed under a Creative Commons Attribution-NonCommercial 3.0 Unported Licence.

J. Jacob-Hirsch, N. Amariglio, M. Kupiec, R. Sorek and G. Rechavi, *Nature*, 2012, **485**, 201–206.
2 K. D. Meyer, Y. Saletore, P. Zumbo, O. Elemento, C. E. Mason and S. R. Jaffrey, *Cell*, 2012, **149**, 1635–1646.
3 B. Linder, A. V. Grozhik, A. O. Olarerin-George, C. Meydan, C. E. Mason and S. R. Jaffrey, *Nat. Methods*, 2015, **12**, 767–772.
4 Y. Fu, D. Dominissini, G. Rechavi and C. He, *Nat. Rev. Genet.*, 2014, **15**, 293–306.
5 K. D. Meyer and S. R. Jaffrey, *Nat. Rev. Mol. Cell Biol.*, 2014, **15**, 313–326.
6 X. Wang, Z. Lu, A. Gomez, G. C. Hon, Y. Yue, D. Han, Y. Fu, M. Parisien, Q. Dai, G. Jia, B. Ren, T. Pan and C. He, *Nature*, 2014, **505**, 117–120.
7 X. Zhao, Y. Yang, B.-F. Sun, Y. Shi, X. Yang, W. Xiao, Y.-J. Hao, X.-L. Ping, Y.-S. Chen, W.-J. Wang, K.-X. Jin, X. Wang, C.-M. Huang, Y. Fu, X.-M. Ge, S.-H. Song, H. S. Jeong, H. Yanagisawa, Y. Niu, G.-F. Jia, W. Wu, W.-M. Tong, A. Okamoto, C. He, J. M. R. Danielsen, X.-J. Wang and Y.-G. Yang, *Cell Res.*, 2014, **24**, 1403–1419.
8 Y. Wang, Y. Li, J. I. Toth, M. D. Petroski, Z. Zhang and J. C. Zhao, *Nat. Cell Biol.*, 2014, **16**, 191–198.
9 X. Wang, B. S. Zhao, I. A. Roundtree, Z. Lu, D. Han, H. Ma, X. Weng, K. Chen, H. Shi and C. He, *Cell*, 2015, **161**, 1388–1399.
10 M. Bartosovic, H. C. Molares, P. Gregorova, D. Hrossova, G. Kudla and S. Vanacova, *Nucleic Acids Res.*, 2017, **45**, 11356–11370.
11 J. Liu, Y. Yue, D. Han, X. Wang, Y. Fu, L. Zhang, G. Jia, M. Yu, Z. Lu, X. Deng, Q. Dai, W. Chen and C. He, *Nat. Chem. Biol.*, 2014, **10**, 93–95.
12 X. Wang, J. Feng, Y. Xue, Z. Guan, D. Zhang, Z. Liu, Z. Gong, Q. Wang, J. Huang, C. Tang, T. Zou and P. Yin, *Nature*, 2016, **534**, 575–578.
13 P. Wang, K. A. Doxtader and Y. Nam, *Mol. Cell*, 2016, **63**, 306–317.
14 G. Jia, Y. Fu, X. Zhao, Q. Dai, G. Zheng, Y. Yang, C. Yi, T. Lindahl, T. Pan, Y.-G. Yang and C. He, *Nat. Chem. Biol.*, 2011, **7**, 885–887.
15 G. Zheng, J. A. Dahl, Y. Niu, P. Fedorcsak, C.-M. Huang, C. J. Li, C. B. Vågbø, Y. Shi, W.-L. Wang, S.-H. Song, Z. Lu, R. P. G. Bosmans, Q. Dai, Y.-J. Hao, X. Yang, W.-M. Zhao, W.-M. Tong, X.-J. Wang, F. Bogdan, K. Furu, Y. Fu, G. Jia, X. Zhao, J. Liu, H. E. Krokan, A. Klungland, Y.-G. Yang and C. He, *Mol. Cell*, 2013, **49**, 18–29.
16 T. Gerken, C. A. Girard, Y.-C. L. Tung, C. J. Webby, V. Saudek, K. S. Hewitson, G. S. H. Yeo, M. A. McDonough, S. Cunliffe, L. A. McNeill, J. Galvanovskis, P. Rorsman, P. Robins, X. Prieur, A. P. Coll, M. Ma, Z. Jovanovic, I. S. Farooqi, B. Sedgwick, I. Barroso, T. Lindahl, C. P. Ponting, F. M. Ashcroft, S. O'Rahilly and C. J. Schofield, *Science*, 2007, **318**, 1469–1472.
17 B. I. Fedeles, V. Singh, J. C. Delaney, D. Li and J. M. Essigmann, *J. Biol. Chem.*, 2015, **290**, 20734–20742.
18 C. Schofield and R. Hausinger, *2-Oxoglutarate-Dependent Oxygenases*, Royal Society of Chemistry, Cambridge, 2015.
19 T. M. Frayling, N. J. Timpson, M. N. Weedon, E. Zeggini, R. M. Freathy, C. M. Lindgren, J. R. B. Perry, K. S. Elliott, H. Lango, N. W. Rayner, B. Shields, L. W. Harries, J. C. Barrett, S. Ellard, C. J. Groves, B. Knight, A.-M. Patch, A. R. Ness, S. Ebrahim, D. A. Lawlor, S. M. Ring, Y. Ben-Shlomo, M.-R. Jarvelin, U. Sovio, A. J. Bennett, D. Melzer, L. Ferrucci, R. J. F. Loos, I. Barroso, N. J. Wareham, F. Karpe, K. R. Owen, L. R. Cardon, M. Walker, G. A. Hitman, C. N. A. Palmer, A. S. F. Doney, A. D. Morris, G. D. Smith, A. T. Hattersley and M. I. McCarthy, *Science*, 2007, **316**, 889–894.
20 R. M. Freathy, N. J. Timpson, D. A. Lawlor, A. Pouta, Y. Ben-Shlomo, A. Ruokonen, S. Ebrahim, B. Shields, E. Zeggini, M. N. Weedon, C. M. Lindgren, H. Lango, D. Melzer, L. Ferrucci, G. Paolisso, M. J. Neville, F. Karpe, C. N. A. Palmer, A. D. Morris, P. Elliott, M.-R. Jarvelin, G. D. Smith, M. I. McCarthy, A. T. Hattersley and T. M. Frayling, *Diabetes*, 2008, **57**, 1419–1426.
21 A. Lim, J. Zhou, R. A. Sinha, B. K. Singh, S. Ghosh, K.-H. Lim, P. K.-H. Chow, E. C. Y. Woon and P. M. Yen, *Biochem. Biophys. Res. Commun.*, 2016, **479**, 476–481.
22 C. Graff, L. Keller, W. Xu, H.-X. Wang, B. Winblad and L. Fratiglioni, *Alzheimer's Dementia*, 2010, **6**, S111.
23 C. Tang, R. Klukovich, H. Peng, Z. Wang, T. Yu, Y. Zhang, H. Zheng, A. Klungland and W. Yan, *Proc. Natl. Acad. Sci. U. S. A.*, 2018, **115**, E325–E333.
24 B. Chen, F. Ye, L. Yu, G. Jia, X. Huang, X. Zhang, S. Peng, K. Chen, M. Wang, S. Gong, R. Zhang, J. Yin, H. Li, Y. Yang, H. Liu, J. Zhang, H. Zhang, A. Zhang, H. Jiang, C. Luo and C.-G. Yang, *J. Am. Chem. Soc.*, 2012, **134**, 17963–17971.
25 J. D. W. Toh, L. Sun, L. Z. M. Lau, J. Tan, J. J. A. Low, C. W. Q. Tang, E. J. Y. Cheong, M. J. H. Tan, Y. Chen, W. Hong, Y.-G. Gao and E. C. Y. Woon, *Chem. Sci.*, 2015, **6**, 112–122.
26 Y. Huang, J. Yan, Q. Li, J. Li, S. Gong, H. Zhou, J. Gan, H. Jiang, G.-F. Jia, C. Luo and C.-G. Yang, *Nucleic Acids Res.*, 2015, **43**, 373–384.
27 N. Svensen and S. R. Jaffrey, *Cell Chem. Biol.*, 2016, **23**, 415–425.
28 M. Imanishi, S. Tsuji, A. Suda and S. Futaki, *Chem. Commun.*, 2017, **53**, 12930–12933.
29 S. Zou, J. D. W. Toh, K. H. Q. Wong, Y.-G. Gao, W. Hong and E. C. Y. Woon, *Sci. Rep.*, 2016, **6**, 25677.
30 J. D. Engel and P. H. J. von Hippel, *Biol. Chem.*, 1978, **253**, 927–934.
31 R. Micura, W. Pils, C. Höbartner, K. Grubmayr, M. O. Ebert and B. Jaun, *Nucleic Acids Res.*, 2001, **29**, 3997–4005.
32 E. Kierzek and R. Kierzek, *Nucleic Acids Res.*, 2003, **31**, 4472–4480.
33 C. Roost, S. R. Lynch, P. J. Batista, K. Qu, H. Y. Chang and E. T. Kool, *J. Am. Chem. Soc.*, 2015, **137**, 2107–2115.
34 N. Liu, Q. Dai, G. Zheng, C. He, M. Parisien and T. Pan, *Nature*, 2015, **518**, 560–564.
35 K. I. Zhou, M. Parisien, Q. Dai, N. Liu, L. Diatchenko, J. R. Sachleben and T. Pan, *J. Mol. Biol.*, 2016, **428**, 822–833.

 This journal is © The Royal Society of Chemistry 2018

Open Access Article. Published on 07 August 2018. Downloaded on 7/8/2025 12:55:09 PM.
This article is licensed under a Creative Commons Attribution-NonCommercial 3.0 Unported Licence.

36 K. Yamana, R. Iwase, S. Furutani, H. Tsuchida, H. Zako, T. Yamaoka and A. Murakami, *Nucleic Acids Res.*, 1999, **27**, 2387–2392.
37 M. Nakamura, Y. Fukunaga, K. Sasa, Y. Ohtoshi, K. Kanaori, H. Hayashi, H. Nakano and K. Yamana, *Nucleic Acids Res.*, 2005, **33**, 5887–5895.
38 M. E. Østergaard, P. Cheguru, M. R. Papasani, R. A. Hill and P. J. Hrdlicka, *J. Am. Chem. Soc.*, 2010, **132**, 14221–14228.
39 Y. Park, D. Nim-anussornkul, T. Vilaivan, T. Morii and B. H. Kim, *Bioorg. Med. Chem. Lett.*, 2018, **28**, 77–80.
40 T. Yang, A. Cheong, X. Mai, S. Zou and E. C. Y. Woon, *Chem. Commun.*, 2016, **52**, 6181–6184.
41 C.-G. Yang, C. Yi, E. M. Duguid, C. T. Sullivan, X. Jian, P. A. Rice and C. He, *Nature*, 2008, **452**, 961–965.
42 T. Duncan, S. C. Trewick, P. Koivisto, P. A. Bates, T. Lindahl and B. Sedgwick, *Proc. Natl. Acad. Sci. U. S. A.*, 2002, **99**, 16660–16665.
43 P. A. Aas, M. Otterlei, P. Ø. Falnes, C. B. Vågbø, F. Skorpen, M. Akbari, O. Sundheim, M. Bjørås, G. Slupphaug, E. Seeberg and H. E. Krokan, *Nature*, 2003, **421**, 859–863.
44 O. Sundheim, C. B. Vågbø, M. Bjørås, M. M. L. Sousa, V. Talstad, P. A. Aas, F. Drabløs, H. E. Krokan, J. A. Tainer and G. Slupphaug, *EMBO J.*, 2006, **25**, 3389–3397.
45 W. Aik, J. S. Scotti, H. Choi, L. Gong, M. Demetriades, C. J. Schofield and M. A. McDonough, *Nucleic Acids Res.*, 2014, **42**, 4741–4754.
46 J. Mauer, X. Luo, A. Blanjoie, X. Jiao, A. V. Grozhik, D. P. Patil, B. Linder, B. F. Pickering, J.-J. Vasseur, Q. Chen, S. S. Gross, O. Elemento, F. Debart, M. Kiledjian and S. R. Jaffrey, *Nature*, 2017, **541**, 371–375.
47 S. Hussain, A. A. Sajini, S. Blanco, S. Dietmann, P. Lombard, Y. Sugimoto, M. Paramor, J. G. Gleeson, D. T. Odom, J. Ule and M. Frye, *Cell Rep.*, 2013, **4**, 255–261.
48 V. Khoddami and B. R. Cairns, *Nat. Biotechnol.*, 2013, **31**, 458–464.
49 A. Jeltsch, A. Ehrenhofer-Murray, T. P. Jurkowski, F. Lyko, G. Reuter, S. Ankri, W. Nellen, M. Schaefer and M. Helm, *RNA Biol.*, 2017, **14**, 1108–1123.
50 M. Das, T. Yang, J. Dong, F. Prasetya, Y. Xie, K. Wong, A. Cheong and E. C. Y. Woon, *Chem.–Asian J.*, 2018, DOI: 10.1002/asia.201800729.
51 J.-H. Zhang, T. D. Chung and K. R. Oldenburg, *J. Biomol. Screening*, 1999, **4**, 67–73.
52 I. Walev, S. C. Bhakdi, F. Hofmann, N. Djonder, A. Valeva, K. Aktories and S. Bhakdi, *Proc. Natl. Acad. Sci. U. S. A.*, 2001, **98**, 3185–3190.
53 P. Gulati, E. Avezov, M. Ma, R. Antrobus, P. Lehner, S. O'Rahilly and G. S. H. Yeo, *Biosci. Rep.*, 2014, **34**, 621–628.
54 P. Gulati, M. K. Cheung, R. Antrobus, C. D. Church, H. P. Harding, Y.-C. L. Tung, D. Rimmington, M. Ma, D. Ron, P. J. Lehner, F. M. Ashcroft, R. D. Cox, A. P. Coll, S. O'Rahilly and G. S. H. Yeo, *Proc. Natl. Acad. Sci. U. S. A.*, 2013, **110**, 2557–2562.
55 A. Aas, P. Isakson, C. Bindesbøll, E. A. Alemu, A. Klungland and A. Simonsen, *PLoS One*, 2017, **12**, e0168182.
56 A. Klungland, J. A. Dahl, G. Greggains, P. Fedorcsak and A. Filipczyk, *Nat. Methods*, 2017, **14**, 18–22.
57 J. Zhou, J. Wan, X. Gao, X. Zhang, S. R. Jaffrey and S.-B. Qian, *Nature*, 2015, **526**, 591–594.
58 Y. Xiang, B. Laurent, C.-H. Hsu, S. Nachtergaele, Z. Lu, W. Sheng, C. Xu, H. Chen, J. Ouyang, S. Wang, D. Ling, P.-H. Hsu, L. Zou, A. Jambhekar, C. He and Y. Shi, *Nature*, 2017, **543**, 573–576.
59 Q. Cui, H. Shi, P. Ye, L. Li, Q. Qu, G. Sun, G. Sun, Z. Lu, Y. Huang, C.-G. Yang, A. D. Riggs, C. He and Y. Shi, *Cell Rep.*, 2017, **18**, 2622–2634.
60 M. Engel, S. Roeh, C. Eggert, P. M. Kaplick, L. Tietze, J. Arloth, P. Weber, M. Rex-Haffner, M. Jakovcevski, M. Uhr, M. Eder, C. T. Wotjak, M. V. Schmidt, J. M. Deussing, E. B. Binder and A. Chen, bioRxiv, 2017, 200402.
61 D. Dominissini, S. Nachtergaele, S. Moshitch-Moshkovitz, E. Peer, N. Kol, M. S. Ben-Haim, Q. Dai, A. Di Segni, M. Salmon-Divon, W. C. Clark, G. Zheng, T. Pan, O. Solomon, E. Eyal, V. Hershkovitz, D. Han, L. C. Doré, N. Amariglio, G. Rechavi and C. He, *Nature*, 2016, **530**, 441–446.
62 H. Zhou, I. J. Kimsey, E. N. Nikolova, B. Sathyamoorthy, G. Grazioli, J. McSally, T. Bai, C. H. Wunderlich, C. Kreutz, I. Andricioaei and H. M. Al-Hashimi, *Nat. Struct. Mol. Biol.*, 2016, **23**, 803–810.
63 J. C. Delaney and J. M. Essigmann, *Proc. Natl. Acad. Sci. U. S. A.*, 2004, **101**, 14051–14056.